

RIS-Assisted Joint Sensing and Communications via Fractionally Constrained Fractional Programming

Yiming Liu, *Graduate Student Member, IEEE*, Kareem M. Attiah, and Wei Yu, *Fellow, IEEE*

Abstract—This paper studies an uplink dual-functional sensing and communication system aided by a reconfigurable intelligent surface (RIS), whose reflection pattern is optimally configured to trade-off sensing and communication functionalities. Specifically, the Bayesian Cramér-Rao lower bound (BCRLB) for estimating the azimuth angle of a sensing user is minimized while ensuring the signal-to-interference-plus-noise ratio constraints for communication users. We show that this problem can be formulated as a novel fractionally constrained fractional programming (FCFP) problem. To deal with this highly nontrivial problem, we extend a quadratic transform technique, originally proposed to handle optimization problems containing ratio structures only in objectives, to the scenario where the constraints also contain ratio structures. First, we consider the case where the fading coefficient is known. Using the quadratic transform, the FCFP problem is turned into a sequence of subproblems that are convex except for the constant-modulus constraints which can be tackled using a penalty-based method. To further reduce the computational complexity, we leverage the constant-modulus conditions and propose a novel linear transform. This new transform enables the FCFP problem to be turned into a sequence of linear programming (LP) subproblems, which can be solved with linear complexity in the dimension of reflecting elements. Then, we consider the case where the fading coefficient is unknown. A modified BCRLB is used to make the problem more tractable, and the proposed quadratic transform-based algorithm is used to solve the problem. Finally, numerical results unveil nontrivial and effective reflection patterns that the RIS can be configured to generate to facilitate both functionalities.

Index Terms—Reconfigurable intelligent surface (RIS), uplink, joint sensing and communications, beamforming, fractional programming, Bayesian Cramér-Rao lower bound (BCRLB).

I. INTRODUCTION

WITH the increasing demands on positioning information and for sensing functionality in the beyond-fifth-generation (B5G) and six-generation (6G) wireless networks, integrated sensing and communications (ISAC) is viewed as a promising use case for future networks (see, e.g., [2] and the references therein), particularly when operating at the millimeter-wave (mmWave) and terahertz (THz) bands [3], [4]. However, signal propagation characteristics at these high frequencies are challenging for both sensing and communications due to the penetrating pathloss. In particular, due to obstacles that are often present in practical scenarios, sensing and/or communications users are often located in regions with

no direct line-of-sight (LoS) paths from the base station (BS), but the non-line-of-sight (NLoS) paths are often too weak to ensure good performance.

To address this issue, reconfigurable intelligent surface (RIS) [5], also known as intelligent reflecting surface (IRS) [6], has emerged as a viable and promising solution for undertaking sensing and communication tasks in regions with no direct LoS paths. Specifically, RIS is a cost-effective planar reflector capable of altering the phases of incident electromagnetic (EM) waves with very low power consumption. It has the ability to generate controllable and desired reflection patterns, and to create new LoS paths, in order to enable joint sensing and communications in practical deployment scenarios with many obstructions [7].

This paper investigates an *uplink* RIS-assisted joint sensing and communications problem, where the direct paths between the users and the BS are blocked and the reflection patterns of the RIS need to be optimally configured in order to serve both sensing and communication purposes. Specifically, the sensing user actively transmits pilots to the BS through the RIS, allowing the BS to estimate the channel characteristics of the sensing user based on the received pilots. At the same time, the communication users transmit data symbols to the BS through the RIS. In this paper, we separate the sensing and communication users spatially via BS and RIS beamforming. This is possible, because the numbers of BS antennas and RIS elements typically exceed the number of users.

Unlike conventional radar-based downlink sensing, pilot-based uplink sensing enables the sensing users to autonomously determine the timing and necessity of initiating sensing services; they only actively transmit pilots when sensing services are needed. In addition, uplink sensing also helps conserve BS resources and reduce the burden on the BS.

There are many prior works investigating joint sensing and communications with/without the assistance of RIS [8]–[21]. For example, the authors in [8] design the beampatterns for a dual-functional radar-communication system aiming to achieve a flexible tradeoff between two functionalities. To facilitate the MIMO radar in utilizing its full degree-of-freedom (DoF), the authors in [9] jointly design the individual radar and communication waveforms to optimize both the radar beampattern and the signal-to-interference-and-noise ratio (SINR) for the communication users. In [10], the authors consider an RIS-enabled target estimation, where dedicated sensors are installed at the RIS for estimating the directions of nearby targets. In [11]–[13], the authors investigate RIS-enabled target detection, where the RIS beamformer is designed to maximize the target detection probability. In [14]–[16], the authors study an RIS-

The authors are with The Edward S. Rogers Sr. Department of Electrical and Computer Engineering, University of Toronto, Toronto, Ontario M5S 3G4, Canada (e-mail: eceym.liu@mail.utoronto.ca; weiyu@ece.utoronto.ca). (Corresponding author: Wei Yu.)

This work was supported by an NSERC Discovery Grant. The materials in this paper have been presented in part at the IEEE Global Communications Conference, Cape Town, South Africa, 2024 [1].

assisted ISAC system, where the beamformers are designed to maximize the SNR for sensing while satisfying certain quality-of-service (QoS) constraints. The sensing metrics adopted in these aforementioned works, e.g., SNR maximization and beam patterns matching, are all based on heuristics.

The Cramér-Rao lower bound (CRLB) is another widely-adopted metric for sensing performance, because it provides a lower bound on the mean-squared error (MSE) for parameter estimation among all unbiased estimators. For example, [19] utilizes the CRLB to evaluate the target estimation performance in a system without RIS. In [20], the CRLB for an RIS-aided wireless sensing system is minimized, although communication functions are not integrated into the system. In [21], the authors further incorporate the communication function based on the prior work in [20].

It should be noted that the standard CRLB depends on the actual values of the parameters to be estimated (such as the angles-of-arrival and the channel fading coefficients), which are unknown in practice. A more practical approach is to assume a prior distribution of the parameters to be estimated and to adopt the Bayesian CRLB (BCRLB) (e.g., [22]) as a more suitable sensing metric.

In this paper, we investigate an RIS-assisted dual-functional uplink sensing and communication system, where the beamformer at the RIS is designed to balance the tradeoff between the two functions. We deal with a specific problem of minimizing the BCRLB for an angle estimation problem with one sensing user and multiple communication users under SINR constraints. Different from radar-based downlink ISAC, where the sensing signals are received at the BS and the communication signals are received at the user side, in the uplink case, both the sensing and the communication signals are transmitted from the users through the RIS and received at the BS. Because of the interference among the user signals, we show in this paper that the uplink joint sensing and communications problem leads to a novel fractionally constrained fractional programming (FCFP) problem formulation with extra RIS amplitude constraints.

To solve this nontrivial optimization problem, we extend a quadratic transform technique, previously proposed to handle optimization problems for which the objective function has a fractional structure [23], to the scenario where the constraints also contain ratio terms. We first consider the problem in the case of known fading coefficient. We show that the quadratic transform allows the original problem to be transformed into a sequence of subproblems which are convex except for the extra constant-modulus constraints introduced by the RIS. A penalty-based method is then used to handle the constant-modulus constraints. To further reduce the complexity, we leverage the constant-modulus condition and propose a new transform called the constant-modulus linear transform. This new technique allows the FCFP problem to be transformed into a sequence of linear programming (LP) subproblems, which can be solved with linear complexity in the dimension of reflecting elements.

We also consider the case of unknown fading coefficient. In this scenario, a more complicated problem is formulated with a modified BCRLB. The quadratic transform technique

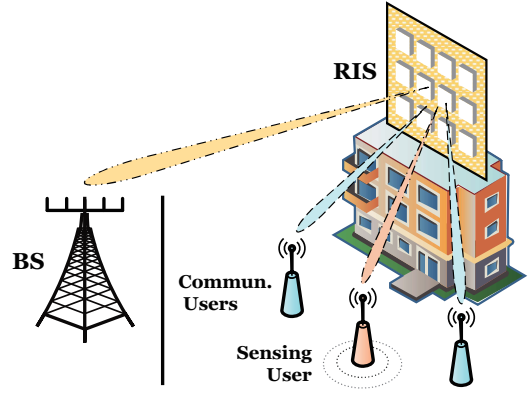


Fig. 1. An uplink RIS-assisted joint sensing and communication system.

and the penalty-based method can also be used to solve this problem. Numerical results demonstrate the effectiveness of the proposed algorithms and show that the optimization can produce nontrivial RIS reflection patterns that facilitate both sensing and communication functionalities at the same time.

II. SYSTEM AND SIGNAL MODEL

A. Channel Model

Consider an uplink RIS-assisted dual-functional sensing and communication system, where a BS with M antennas intends to estimate the azimuth angle from the sensing user to the RIS, while simultaneously providing communication services to K single-antenna users, as illustrated in Fig. 1.

The RIS performs a linear mapping from the incident signal vector to a reflected signal vector, which can be modeled by a multiplication with an equivalent diagonal phase-shift matrix $\text{diag}\{\mathbf{x}\}$. The vector \mathbf{x} represents the reflecting coefficients of the RIS and is expressed as

$$\mathbf{x} = [e^{j\theta_1}, e^{j\theta_2}, \dots, e^{j\theta_N}]^T, \quad (1)$$

where $\theta_n \in [-\pi, \pi)$ denotes the phase shift of the n -th element of the RIS, $n = 1, \dots, N$, and $N = N_{\text{row}} \times N_{\text{col}}$ is the number of reflecting elements in the RIS. In this paper, we design \mathbf{x} to enable joint sensing and communications. Note that in this model of RIS beamforming, the optimizing variable \mathbf{x} has a constant-modulus constraint, i.e., $|x_n| = 1, \forall n$, which may be a challenging constraint to handle.

We assume that all the direct channels between the users and the BS are obstructed. Thus, the radio propagation paths can only be constructed through the cascaded reflecting channels. The ability to help establish links in situations where the direct channels are obstructed is one of the crucial advantages of RIS.

The channel matrix from the RIS to the BS, which is shared by all sensing and communications users, is represented by \mathbf{G} and is assumed to be known at the BS. This assumption is reasonable owing to the fixed positions of the BS and the RIS, as well as the availability of proper channel estimation methods (see, e.g., [24] and the references therein).

For simplicity, the channel from each user to the RIS is assumed to contain only one dominant LoS path¹. Furthermore, the array response of the RIS is assumed to be a function of only the azimuth angle of the path. In other words, the sensing user is assumed to be located in a two-dimensional plane with a fixed elevation angle, so that the overall array response of the uniform rectangular array of RIS elements depends only on the sensing user's azimuth angle-of-arrival (AoA) η as follows:

$$\mathbf{v}(\eta) = \left[e^{j\tau \cos(\eta)v(1)}, \dots, e^{j\tau \cos(\eta)v(N)} \right]^T, \quad (2)$$

where $\tau = 2\pi d/\omega$, and ω denotes the carrier wavelength, d is the spacing between the reflecting elements (typically at half wavelength), and $v(n) = \text{mod}(n-1, N_{\text{col}})$. In this case, the cascaded reflecting channel from the sensing user to the BS through the RIS becomes

$$\mathbf{u} = \mathbf{G} \text{diag}\{\mathbf{x}\} \alpha \mathbf{v}(\eta) = \alpha \mathbf{G} \text{diag}\{\mathbf{v}(\eta)\} \mathbf{x} \triangleq \alpha \mathbf{U}(\eta) \mathbf{x}, \quad (3)$$

where α denotes the complex fading coefficient of the channel between the sensing user and the RIS. The sensing task considered in this paper is for the BS to estimate the azimuth angle η of the sensing user.

Likewise, let ϕ_k denote the azimuth AoA of the k -th communication user at the RIS. The cascaded reflecting channel of the k -th communication user can similarly be expressed as

$$\mathbf{h}_k = \beta_k \mathbf{G} \text{diag}\{\mathbf{v}(\phi_k)\} \mathbf{x} \triangleq \mathbf{H}_k \mathbf{x}, \quad (4)$$

where β_k denotes the complex fading coefficient of the channel between the communication user and the RIS. In this paper, we assume that the communication channels \mathbf{H}_k can be estimated perfectly at the BS.

B. Signal Model for Joint Sensing and Communications

This paper considers the following joint sensing and communications scenario. Within the channel coherence time T , the K communication users transmit data symbols $c_1(t), \dots, c_K(t)$, respectively, for $t = 1, \dots, T$, and the data symbols are modeled as independent and identically distributed (i.i.d.) Gaussian random variables obeying $\mathcal{CN}(0, p_k)$, where p_k is the fixed transmit power of the k -th communication user, $k = 1, \dots, K$. In the meanwhile, the sensing user also transmits a sequence of known pilots $s(t)$ of fixed power p synchronously to the BS, for $t = 1, \dots, T$.

Based on the channel model established in the previous section, the received signal at the BS can be expressed as

$$\mathbf{y}(t) = \alpha \mathbf{U}(\eta) \mathbf{x}(t) s(t) + \sum_{k=1}^K \mathbf{H}_k \mathbf{x}(t) c_k(t) + \mathbf{n}(t), \quad (5)$$

for $t = 1, \dots, T$, where $\mathbf{n}(t)$ represents the additive white Gaussian noise distributed as $\mathcal{CN}(\mathbf{0}, \sigma_n^2 \mathbf{I})$.

This paper aims to design the RIS reflection coefficients in order to enable joint sensing and communications. This is done by adaptively setting $\mathbf{x}(t)$ in each symbol period t .

¹The mmWave channel can often be modeled by a dominant LoS path [25]. As RIS is often deployed in close proximity to the user side, we only consider the dominant LoS path in the user-RIS link. However, this work is applicable more generally to the case where the user-RIS links are modeled as a Rician fading channel.

Specifically, we assume that the sensing operation takes place in one symbol period at a time. The optimization process aims to design the RIS coefficients to minimize the estimation error for sensing η in the next symbol period, while ensuring communication performance is maintained. The adaptation of $\mathbf{x}(t)$ is based on the effective channels of the communication users \mathbf{H}_k , the channel model for the sensing user $\alpha \mathbf{U}(\eta)$, as well as the prior knowledge of unknown parameters η and α .

This paper assumes that the numbers of BS antennas and RIS elements exceed the number of served users and rely on beamforming at the RIS and at the BS to spatially separate the sensing and communication users. We assume that no interference cancellation is performed at the BS. Although interference cancellation can further improve performance, it comes at a cost of increased complexity and delay, because it would require the completion of one task (e.g., estimating sensing angles or detecting data symbols) before starting of the next task. In contrast, separating the user in the spatial domain allows the sensing and all the communication tasks to be performed simultaneously.

III. SENSING AND COMMUNICATION PERFORMANCE METRICS AND PROBLEM FORMULATION

In this section, we establish the performance metrics of both sensing and communications. Specifically, We use the BCRLB as a metric of sensing performance, while adopting the SINR as a measure of communication quality. Based on the two established metrics, we formulate the optimization problem for the task of joint sensing and communications. For simplicity, the fading coefficient α is assumed to be known for now. The scenario where α is unknown, so that both α and η are required to be estimated, is considered later in this paper.

A. Performance Metric for Sensing

We first derive the classic CRLB, then present its Bayesian version, i.e., the BCRLB, as a metric for sensing. Let $\hat{\eta}$ be an unbiased estimator of η over one symbol period. According to the Cramér-Rao theorem [26], the mean square error (MSE) of any unbiased estimator for η is bounded from below as

$$\mathbb{E}|\hat{\eta} - \eta|^2 \geq \text{CRLB}(\eta) \triangleq \frac{1}{\text{FI}(\eta)}, \quad (6)$$

where $\text{FI}(\eta)$ is the Fisher information, defined as

$$\text{FI}(\eta) \triangleq \mathbb{E} \left[\left(\frac{\partial \ln \mathcal{L}(\mathbf{y}; \eta)}{\partial \eta} \right)^2 \right], \quad (7)$$

and $\mathcal{L}(\mathbf{y}; \eta)$ is the likelihood function of \mathbf{y} as function of η . Since the pilot signal from the sensing user is known, and both the communication signals and the noise are modeled as Gaussian random vectors, $\mathcal{L}(\mathbf{y}; \eta)$ is the probability density function of a Gaussian distribution with the mean and the covariance matrix given as below:

$$\text{mean}(\mathbf{y} | \eta) = \alpha \mathbf{U}(\eta) \mathbf{x} s, \quad (8)$$

$$\text{Cov}(\mathbf{y} | \eta) = \sum_{k=1}^K p_k (\mathbf{H}_k \mathbf{x}) (\mathbf{H}_k \mathbf{x})^H + \sigma_n^2 \mathbf{I} \triangleq \Sigma^0(\mathbf{x}). \quad (9)$$

Then, the Fisher information $\text{FI}(\eta)$ can be expressed as [18]

$$\text{FI}(\eta) = 2 \left\{ \left(\alpha \dot{\mathbf{U}}(\eta) \mathbf{x} \right)^H (\boldsymbol{\Sigma}^0(\mathbf{x}))^{-1} \left(\alpha \dot{\mathbf{U}}(\eta) \mathbf{x} \right) \right\}, \quad (10)$$

where $\dot{\mathbf{U}}(\eta)$ denotes the derivative of $\mathbf{U}(\eta)$ with respect to η .

Note here that we drop the time index t , because we consider the sensing operation over one symbol period only. The derivation can be easily extended to case where sensing takes place over multiple symbol periods.

One can observe that $\text{FI}(\eta)$ has a fractional structure with respect to \mathbf{x} , attributed to the fact that both the sensing and communication signals propagate through the RIS and interact with each other at the BS. In particular, the communication signals are regarded as interference for sensing, because sensing and communication are assumed to take place simultaneously without interference cancellation.

CRLB has been widely used to characterize the performance for parameter estimation; it is an alternative metric to the MSE when the MSE is difficult to compute. However, it can be seen from (10) that the computation of CRLB depends on the exact values of the parameters to be estimated, which are unknown. Consequently, we cannot directly employ this classic CRLB.

To address this issue, we assume a prior distribution of the parameters of interest and adopt the Bayesian version BCRLB to evaluate sensing performance [27], [28]. The prior distribution can be updated based on successive observations.

Following the derivations in [29], [30], the BCRLB of η with a prior distribution $q(\eta)$ can be expressed as follows:

$$\text{BCRLB}(\eta) = \frac{1}{\mathbb{E}_{q(\eta)}[\text{FI}(\eta)] + \text{FIP}(\eta)}, \quad (11)$$

where $\text{FIP}(\eta)$ is the Fisher information of the prior itself and is independent of the optimization variable \mathbf{x} . One can observe from (11) that minimizing the BCRLB over \mathbf{x} is equivalent to maximizing the following new metric:

$$\begin{aligned} \mathcal{A} &\triangleq \frac{\mathbb{E}_{q(\eta)}[\text{FI}(\eta)]}{2p|\alpha|^2} \\ &= \mathbb{E}_{q(\eta)} \left[\left(\dot{\mathbf{U}}(\eta) \mathbf{x} \right)^H (\boldsymbol{\Sigma}^0(\mathbf{x}))^{-1} \left(\dot{\mathbf{U}}(\eta) \mathbf{x} \right) \right]. \end{aligned} \quad (12)$$

However, computing \mathcal{A} still requires an integration with respect to $q(\eta)$. The theorem below extracts \mathbf{x} from the integral.

Theorem 1: Consider a second moment matrix defined as

$$\dot{\mathbf{R}} = \mathbb{E}_{q(\eta)} \left[\text{vec} \left(\dot{\mathbf{U}}(\eta) \right) \text{vec}^H \left(\dot{\mathbf{U}}(\eta) \right) \right], \quad (13)$$

where $\text{vec}(\cdot)$ is the vectorization operation. Let the eigendecomposition of this matrix be

$$\dot{\mathbf{R}} = \sum_{r=1}^R \kappa_r \mathbf{r}_r \mathbf{r}_r^H. \quad (14)$$

Then, \mathcal{A} can be equivalently rewritten as

$$\mathcal{A} = \sum_{r=1}^R \kappa_r (\mathbf{R}_r \mathbf{x})^H (\boldsymbol{\Sigma}^0(\mathbf{x}))^{-1} (\mathbf{R}_r \mathbf{x}), \quad (15)$$

where $\kappa_r > 0$ and $\mathbf{R}_r = \text{vec}^{-1}(\mathbf{r}_r)$.

Proof: The proof is given in Appendix A. ■

Based on Theorem 1, the metric \mathcal{A} for estimating η can be transformed into a weighted sum of multi-dimensional ratios in \mathbf{x} as (15). Note that the standard CRLB is a special case of the above, where η is deterministic and the prior distribution $q(\eta)$ has zero variance. In this case, $\dot{\mathbf{R}}$ is rank-one, and (15) reduces to (10).

B. Performance Metric for Communications

For the communication users, we use a linear receive beamformer \mathbf{w}_k at the BS to perform detection and demodulation of the data symbol for each uplink user k . Since interference cancellation is not performed at the BS, the pilot signal from the sensing user is regarded as interference to the communication users. Furthermore, because the AoA η is not known, we opt to use the expected power of the pilot signal over its prior distribution $q(\eta)$ as the interference power in the SINR expression. Although strictly speaking, the interference due to an actual realization of η may lead to a higher interference level than the expected interference power, the use of expected interference power leads to a more tractable problem formulation.

With these assumptions, the SINR of the k -th communication user can now be expressed as

$$\gamma_k = \frac{p_k |\mathbf{w}_k^H \mathbf{H}_k \mathbf{x}|^2}{p \mathbb{E}_{q(\eta)} \left[|\alpha \mathbf{w}_k^H \mathbf{U}(\eta) \mathbf{x}|^2 \right] + \sum_{j \neq k} p_j |\mathbf{w}_k^H \mathbf{H}_j \mathbf{x}|^2 + \sigma_n^2}. \quad (16)$$

For a fixed RIS reflecting coefficient \mathbf{x} , optimizing the receive combining vector \mathbf{w}_k to maximize the SINR γ_k is a generalized Rayleigh quotient problem:

$$\underset{\mathbf{w}_k}{\text{maximize}} \quad \frac{p_k \mathbf{w}_k^H \left((\mathbf{H}_k \mathbf{x}) (\mathbf{H}_k \mathbf{x})^H \right) \mathbf{w}_k}{\mathbf{w}_k^H \boldsymbol{\Sigma}_k^c(\mathbf{x}) \mathbf{w}_k}, \quad (17)$$

where $\boldsymbol{\Sigma}_k^c(\mathbf{x})$ is the covariance matrix of the combined interference and noise

$$\begin{aligned} \boldsymbol{\Sigma}_k^c(\mathbf{x}) &= \sum_{j \neq k} p_j (\mathbf{H}_j \mathbf{x}) (\mathbf{H}_j \mathbf{x})^H \\ &\quad + p \mathbb{E}_{q(\eta)} \left[(\alpha \mathbf{U}(\eta) \mathbf{x}) (\alpha \mathbf{U}(\eta) \mathbf{x})^H \right] + \sigma_n^2 \mathbf{I}. \end{aligned} \quad (18)$$

The expectation term in (18) can be rewritten as

$$\begin{aligned} \mathbb{E}_{q(\eta)} \left[(\alpha \mathbf{U}(\eta) \mathbf{x}) (\alpha \mathbf{U}(\eta) \mathbf{x})^H \right] &= \\ \text{vec}^{-1} \left(\mathbb{E}_{q(\eta)} \left[(\alpha \mathbf{U}(\eta))^* \otimes (\alpha \mathbf{U}(\eta)) \right] \text{vec}(\mathbf{x} \mathbf{x}^H) \right), \end{aligned} \quad (19)$$

so \mathbf{x} can be taken out of the expectation operation. The optimal solution \mathbf{w}_k^* can then be found in closed-form as

$$\mathbf{w}_k^* = \left((\boldsymbol{\Sigma}_k^c(\mathbf{x}))^{-1} \mathbf{H}_k \mathbf{x} \right) / \left\| (\boldsymbol{\Sigma}_k^c(\mathbf{x}))^{-1} \mathbf{H}_k \mathbf{x} \right\|_2. \quad (20)$$

With this optimal receive combining vector, the SINR in (16) can be rewritten as a multi-dimensional ratio as

$$\gamma_k = p_k (\mathbf{H}_k \mathbf{x})^H (\boldsymbol{\Sigma}_k^c(\mathbf{x}))^{-1} (\mathbf{H}_k \mathbf{x}). \quad (21)$$

In this paper, we consider the design of receive combiner and RIS reflecting coefficients to ensure that some minimal SINR threshold is satisfied for each user.

C. Problem Formulation

Based on the performance metrics discussed in the previous two sections, the problem of optimally designing the RIS reflecting coefficients for joint sensing and communications can now be formulated as

$$\text{(P1): } \underset{\mathbf{x}}{\text{maximize}} \quad \mathcal{A}(\mathbf{x}) \quad (22a)$$

$$\text{subject to} \quad \gamma_k(\mathbf{x}) \geq \Gamma, \quad \forall k \quad (22b)$$

$$|x_n| = 1, \quad \forall n \quad (22c)$$

where Γ denotes the SINR threshold for the communication users. The threshold value affects a trade-off between the two functionalities. For example, when Γ is zero, the problem reduces to a sensing-only problem.

The above problem formulation assumes a prior $q(\eta)$ and optimizes \mathbf{x} for the next symbol period. This process can be repeated in a sequential fashion within the channel coherence time, so that the RIS reflecting coefficients \mathbf{x} can be adjusted for the subsequent symbols, while the prior distribution $q(\eta)$ is updated to account for the observations made over time.

We note here that when \mathbf{x} is adjusted within the coherence time, the communication receivers can update their knowledge of the effective channels using the model $\mathbf{h}_k = \mathbf{H}_k \mathbf{x}$, so that the symbol detector can be updated accordingly without having to re-estimate the effective channel. The SINR expressions remain valid for the new effective channel.

Throughout this paper, the sensing operation is assumed to take place over one symbol at a time. But the proposed problem formulation can also be readily extended to the case where each sensing operation takes place over multiple symbol periods by modifying the BCRLB expression to be over multiple symbols.

The rest of this paper focuses on solving the problem (P1) in (22). Observe that this problem is a FCFP problem, because it has sum-of-ratios as the objective function (i.e., (15)) and it has fractional constraints (i.e., (21)). In the next two sections, we present two different algorithms to tackle problem (P1).

IV. QUADRATIC TRANSFORM BASED ALGORITHM FOR RIS REFLECTING COEFFICIENT DESIGN

In this section, we consider utilizing the quadratic transform technique and the penalty-based method to solve problem (P1). We first modify the quadratic transform to make it to problems with fractional constraints. Then, we utilize the penalty-based method to deal with the constant-modulus constraints.

A. Quadratic Transform for FCFP

We begin by defining a standard multi-dimensional ratio.

Definition 1: A standard multi-dimensional ratio is a function $\mathbb{C}^N \rightarrow \mathbb{R}_+$ of the form

$$f(\mathbf{x}) \triangleq (\mathbf{A}\mathbf{x})^H (\mathbf{D}(\mathbf{x}))^{-1} (\mathbf{A}\mathbf{x}), \quad (23)$$

where the denominator matrix $\mathbf{D}(\mathbf{x})$ has the form

$$\mathbf{D}(\mathbf{x}) \triangleq \sum_m (\mathbf{B}_m \mathbf{x}) (\mathbf{B}_m \mathbf{x})^H + \mathbf{C}, \quad (24)$$

and the constant matrix \mathbf{C} is positive definite.

In a study of optimization problems involving ratio objective functions [23], the following quadratic transform is proposed as a technique to decouple the numerator and the denominator of a ratio. This result is summarized in the following lemma.

Lemma 1: A lower bound for a standard multi-dimensional ratio function $f(\mathbf{x})$ in (23) is the following:

$$f(\mathbf{x}) \geq 2 \Re\{\boldsymbol{\lambda}^H \mathbf{A}\mathbf{x}\} - \boldsymbol{\lambda}^H \mathbf{D}(\mathbf{x}) \boldsymbol{\lambda} \triangleq \tilde{f}(\mathbf{x}, \boldsymbol{\lambda}), \quad \forall \mathbf{x}, \boldsymbol{\lambda}, \quad (25)$$

with the equality achieved at

$$\boldsymbol{\lambda}^* = (\mathbf{D}(\mathbf{x}))^{-1} \mathbf{A}\mathbf{x}. \quad (26)$$

In this paper, we extend this quadratic transform technique into FCFP problems, where the ratios also appear in the constraints, as shown in the following theorem.

Theorem 2: Consider a multi-dimensional-function-of-ratios maximization problem with constraints in fractional form

$$\underset{\mathbf{x} \in \mathcal{X}}{\text{maximize}} \quad h^o(f_1^o(\mathbf{x}), \dots, f_I^o(\mathbf{x})) \quad (27a)$$

$$\text{subject to} \quad h_k^c(f_{k,1}^c(\mathbf{x}), \dots, f_{k,J}^c(\mathbf{x})) \geq c_k, \quad \forall k, \quad (27b)$$

where h^o is a function $\mathbb{R}^I \rightarrow \mathbb{R}$, h_k^c is a function $\mathbb{R}^J \rightarrow \mathbb{R}$, and both functions are non-decreasing in each component, $f_i^o(\mathbf{x})$ and $f_{k,j}^c(\mathbf{x})$ are standard multi-dimensional ratios of the form (23), and \mathcal{X} is a non-empty set. This problem is equivalent to

$$\underset{\mathbf{x} \in \mathcal{X}, \boldsymbol{\lambda}_i^o, \boldsymbol{\lambda}_j^c}{\text{maximize}} \quad h^o(\tilde{f}_1^o(\mathbf{x}, \boldsymbol{\lambda}_1^o), \dots, \tilde{f}_I^o(\mathbf{x}, \boldsymbol{\lambda}_I^o)) \quad (28a)$$

$$\text{subject to} \quad h_k^c(\tilde{f}_{k,1}^c(\mathbf{x}, \boldsymbol{\lambda}_{k,1}^c), \dots, \tilde{f}_{k,J}^c(\mathbf{x}, \boldsymbol{\lambda}_{k,J}^c)) \geq c_k, \quad \forall k \quad (28b)$$

where the transformed functions $\tilde{f}_i^o(\mathbf{x}, \boldsymbol{\lambda}_i^o)$ and $\tilde{f}_{k,j}^c(\mathbf{x}, \boldsymbol{\lambda}_{k,j}^c)$ are defined as in (25). The optimal $\boldsymbol{\lambda}_i^o$ and $\boldsymbol{\lambda}_{k,j}^c$ are functions of the optimal \mathbf{x} in the form of (26) with their respective $\mathbf{D}(\mathbf{x})$ and \mathbf{A} matrices.

Proof: The proof is given in Appendix B. ■

By applying Theorem 2 to problem (P1), we can obtain the following equivalent problem:

$$\text{(P2): } \underset{\mathbf{x}, \boldsymbol{\lambda}_r^o, \boldsymbol{\lambda}_k^c}{\text{maximize}} \quad \tilde{\mathcal{A}}(\mathbf{x}, \boldsymbol{\lambda}_r^o) \triangleq \sum_{r=1}^R \kappa_r \tilde{f}_r^o(\mathbf{x}, \boldsymbol{\lambda}_r^o) \quad (29a)$$

$$\text{subject to} \quad \tilde{f}_k^c(\mathbf{x}, \boldsymbol{\lambda}_k^c) \geq \Gamma_k, \quad \forall k, \quad (29b)$$

$$|x_n| = 1, \quad \forall n, \quad (29c)$$

where $\Gamma_k = \frac{\Gamma}{p_k}$, and the transformed functions are given by

$$\tilde{f}_r^o(\mathbf{x}, \boldsymbol{\lambda}_r^o) = 2 \Re\{(\boldsymbol{\lambda}_r^o)^H \mathbf{R}_r \mathbf{x}\} - (\boldsymbol{\lambda}_r^o)^H \boldsymbol{\Sigma}^o(\mathbf{x}) \boldsymbol{\lambda}_r^o, \quad (30)$$

$$\tilde{f}_k^c(\mathbf{x}, \boldsymbol{\lambda}_k^c) = 2 \Re\{(\boldsymbol{\lambda}_k^c)^H \mathbf{H}_k \mathbf{x}\} - (\boldsymbol{\lambda}_k^c)^H \boldsymbol{\Sigma}_k^c(\mathbf{x}) \boldsymbol{\lambda}_k^c. \quad (31)$$

Problem (P2) is convex over \mathbf{x} except for the extra constant-modulus constraints (29c). To verify concavity, we first examine the function (30). The first term in (30) is affine in \mathbf{x} ; the second term in (30) can be rewritten as

$$(\boldsymbol{\lambda}_r^o)^H \boldsymbol{\Sigma}^o(\mathbf{x}) \boldsymbol{\lambda}_r^o = \mathbf{x}^H \mathbf{M}_r^o(\boldsymbol{\lambda}_r^o) \mathbf{x} + \sigma_n^2 \|\boldsymbol{\lambda}_r^o\|_2^2, \quad (32)$$

where the coefficient of the quadratic term $\mathbf{M}_r^o(\boldsymbol{\lambda}_r^o)$ is

$$\mathbf{M}_r^o(\boldsymbol{\lambda}_r^o) = \sum_{k=1}^K p_k (\mathbf{H}_k^H \boldsymbol{\lambda}_r^o) (\mathbf{H}_k^H \boldsymbol{\lambda}_r^o)^H. \quad (33)$$

Clearly, $\mathbf{M}_r^o(\boldsymbol{\lambda}_r^o)$ is positive semidefinite. Hence, the function (30) is concave with respect to \mathbf{x} , as

$$\tilde{f}_r^o(\mathbf{x}, \boldsymbol{\lambda}_r^o) = -\mathbf{x}^H \mathbf{M}_r^o(\boldsymbol{\lambda}_r^o) \mathbf{x} + 2 \Re \{ (\boldsymbol{\lambda}_r^o)^H \mathbf{R}_r \mathbf{x} \} - \sigma_n^2 \|\boldsymbol{\lambda}_r^o\|_2^2. \quad (34)$$

Similarly, (31) can be rewritten as

$$\tilde{f}_k^c(\mathbf{x}, \boldsymbol{\lambda}_k^c) = -\mathbf{x}^H \mathbf{M}_k^c(\boldsymbol{\lambda}_k^c) \mathbf{x} + 2 \Re \{ (\boldsymbol{\lambda}_k^c)^H \mathbf{H}_k \mathbf{x} \} - \sigma_n^2 \|\boldsymbol{\lambda}_k^c\|_2^2, \quad (35)$$

where $\mathbf{M}_k^c(\boldsymbol{\lambda}_k^c)$ is positive semidefinite and is given by

$$\mathbf{M}_k^c(\boldsymbol{\lambda}_k^c) = \sum_{j \neq k} p_j (\mathbf{H}_j^H \boldsymbol{\lambda}_k^c) (\mathbf{H}_j^H \boldsymbol{\lambda}_k^c)^H + p \mathbb{E}_{q(\eta)} \left[(\alpha \mathbf{U}^H(\eta) \boldsymbol{\lambda}_k^c) (\alpha \mathbf{U}^H(\eta) \boldsymbol{\lambda}_k^c)^H \right]. \quad (36)$$

The expectation in (36) can be rewritten in a manner similar to (19), such that $\boldsymbol{\lambda}_k^c$ can be extracted from the expectation operation. In the next subsection, we handle the constant-modulus constraints in problem (P2).

B. Penalty-Based Method for Modulus Constraints

To deal with the constant-modulus constraints, we employ a penalty-based method as a heuristic solution. Specifically, we relax the constraints to $|x_n| \leq 1$, $\forall n$, then introduce a penalty term into the objective to encourage the solution to be constant-modulus. By doing so, (P2) is transformed into

$$\underset{\mathbf{x}, \mathbf{z}, \boldsymbol{\lambda}_r^o, \boldsymbol{\lambda}_k^c}{\text{maximize}} \quad \tilde{\mathcal{A}}(\mathbf{x}, \boldsymbol{\lambda}_r^o) - \mu \|\mathbf{x} - \mathbf{z}\|_2^2 \quad (37a)$$

$$\text{subject to} \quad \tilde{f}_k^c(\mathbf{x}, \boldsymbol{\lambda}_k^c) \geq \Gamma_k, \quad \forall k, \quad (37b)$$

$$|x_n| \leq 1, \quad |\hat{x}_n| = 1, \quad \forall n, \quad (37c)$$

where $\mu > 0$ represents the coefficient of the penalty term and the new auxiliary variable \mathbf{z} is unit-modulus. This problem can be solved by iteratively updating the RIS reflecting coefficients and all the other auxiliary variables, as shown in Algorithm 1. Note that we gradually increase μ in an outer loop until the stopping criterion is met.

To show the convergence of the proposed algorithm, we first consider the inner loop, i.e., the algorithm with a fixed μ . The key is that in each iteration of the inner loop, all the auxiliary variables are updated optimally so that both the values of the objective and the constraint functions are *nondecreasing*. Thus, the solution of \mathbf{x} updated in the previous iteration is *feasible* in the current iteration. Furthermore, optimizing \mathbf{x} in (37) with fixed auxiliary variables is a *convex* quadratically constrained quadratic program (QCQP), the optimal solution of which can be easily obtained by an optimization solver, such as the CVX. Hence, the update of \mathbf{x} in the current iteration leads to a non-decreasing objective value, so the inner loop must converge.

In the outer loop, the penalty increases as μ increases, making the solution more likely to satisfy the modulus constraints. However, a larger penalty coefficient μ makes the inner loop to converge more slowly. So we incorporate the outer loop to gradually increase μ . If a penalty coefficient μ is selected so that the penalty term is zero when the algorithm converges, the Karush-Kuhn-Tucker (KKT) conditions on \mathbf{x} for the problem

Algorithm 1 Quadratic Transform and Penalty-Based Method

- 1: Initialize $\mu > 0$.
- 2: Initialize num_iter = 0 and max_iter.
- 3: Initialize \mathbf{x} as a feasible point of the original problem (P1).
- 4: **repeat**
- 5: **repeat**
- 6: Update $\mathbf{z} = \exp[j \arg(\mathbf{x})]$.
- 7: Update $\boldsymbol{\lambda}_r^o = (\boldsymbol{\Sigma}^o(\mathbf{x}))^{-1} \mathbf{R}_r \mathbf{x}$ for all r .
- 8: Update $\boldsymbol{\lambda}_k^c = (\boldsymbol{\Sigma}_k^c(\mathbf{x}))^{-1} \mathbf{H}_k \mathbf{x}$ for all k .
- 9: Optimize \mathbf{x} in (37) with fixed auxiliary variables.
- 10: **until** convergence
- 11: $\mu = \xi \mu$ with $\xi > 1$.
- 12: num_iter = num_iter + 1.
- 13: **until** $\|\mathbf{x} - \mathbf{z}\| = 0$ or num_iter > max_iter.
- 14: Update $\mathbf{x} = \exp[j \arg(\mathbf{x})]$.
- 15: **output** The optimized RIS reflecting coefficients \mathbf{x} .

(37), under the optimal auxiliary variables, must be the same as for the original problem (P1), hence the algorithm must have converged to a KKT point of problem (P1).

The computational complexity of the proposed algorithm in each iteration mainly arises from solving a QCQP problem of updating \mathbf{x} , thus the per-iteration computational complexity of this algorithm is dominated by $\mathcal{O}(KN^3)$.

V. CONSTANT-MODULUS LINEAR TRANSFORM BASED ALGORITHM FOR RIS REFLECTING COEFFICIENT DESIGN

In the previous section, we employ the quadratic transform to deal with the fractional structures and utilize a penalty-based method to handle constant-modulus constraints. However, the computational complexity of solving a QCQP problem in each iteration is non-negligible. Furthermore, to determine a proper penalty coefficient, an extra outer loop is required, which also increases the complexity. To reduce computational complexity, a new transform, called the constant-modulus linear transform, is proposed in this section to solve problem (P1), building upon the quadratic transform and the constant-modulus property.

A. Constant-Modulus Linear Transform

The following lemma is the basis of the new transform.

Lemma 2: A lower bound for a standard multi-dimensional ratio function $f(\mathbf{x})$ in (23) with variable \mathbf{x} being *unit-modulus* can be constructed as

$$f(\mathbf{x}) \geq 2 \Re \{ \mathbf{x}^H ((\delta \mathbf{I} - \mathbf{M}(\boldsymbol{\lambda})) \mathbf{z} + \mathbf{A}^H \boldsymbol{\lambda}) \} + c(\mathbf{z}, \boldsymbol{\lambda}) \triangleq \bar{f}(\mathbf{x}, \mathbf{z}, \boldsymbol{\lambda}), \quad \forall \boldsymbol{\lambda}, \quad \forall \mathbf{x}, \mathbf{z} \in \mathbb{T}^N, \quad (38)$$

where $\mathbb{T} = \{x \in \mathbb{C} \mid |x| = 1\}$, the matrix $\mathbf{M}(\boldsymbol{\lambda})$ is given by

$$\mathbf{M}(\boldsymbol{\lambda}) = \sum_m (\mathbf{B}_m^H \boldsymbol{\lambda}) (\mathbf{B}_m^H \boldsymbol{\lambda})^H, \quad (39)$$

δ is the trace of $\mathbf{M}(\boldsymbol{\lambda})$, and $c(\mathbf{z}, \boldsymbol{\lambda})$ is given by

$$c(\mathbf{z}, \boldsymbol{\lambda}) = \mathbf{z}^H \mathbf{M}(\boldsymbol{\lambda}) \mathbf{z} - 2\delta N - \boldsymbol{\lambda}^H \mathbf{C} \boldsymbol{\lambda}. \quad (40)$$

The equality in (38) is achieved at $\mathbf{z}^* = \mathbf{x}$ and $\boldsymbol{\lambda}^*$ in (26).

Proof: The proof is given in Appendix C. ■

This lemma uses a key technique in [31] that turns a quadratic optimization over \mathbf{x} with unit-modulus constraints into a linear optimization. This is made possible by taking advantage of the unit-modulus property of the variable \mathbf{x} .

Based on Lemma 2, the constant-modulus linear transform, which is proposed for FCFP problems with constant-modulus constraints, can be stated in the following theorem.

Theorem 3: Consider a maximization FCFP problem with constant-modulus constraints

$$\underset{\mathbf{x}}{\text{maximize}} \quad \sum_i w_i f_i^o(\mathbf{x}) \quad (41a)$$

$$\text{subject to} \quad f_j^c(\mathbf{x}) \geq c_j, \quad \forall j, \quad (41b)$$

$$|x_n| = 1, \quad \forall n, \quad (41c)$$

where $w_i > 0$ denotes the weight, $f_i^o(\mathbf{x})$ and $f_j^c(\mathbf{x})$ are multi-dimensional ratio functions of the form (23). This problem is equivalent to

$$\underset{\mathbf{x}, \mathbf{z}, \boldsymbol{\lambda}_i^o, \boldsymbol{\lambda}_j^c}{\text{maximize}} \quad \sum_i w_i \bar{f}_i^o(\mathbf{x}, \mathbf{z}, \boldsymbol{\lambda}_i^o) \quad (42a)$$

$$\text{subject to} \quad \bar{f}_j^c(\mathbf{x}, \mathbf{z}, \boldsymbol{\lambda}_j^c) \geq c_j, \quad \forall j, \quad (42b)$$

$$|x_n| = 1, \quad \forall n, \quad (42c)$$

where the transformed functions $\bar{f}_i^o(\mathbf{x}, \mathbf{z}, \boldsymbol{\lambda}_i^o)$ and $\bar{f}_j^c(\mathbf{x}, \mathbf{z}, \boldsymbol{\lambda}_j^o)$ are defined as in (38). The optimal \mathbf{z} equals to the optimal \mathbf{x} , and the optimal $\boldsymbol{\lambda}_i^o$ and $\boldsymbol{\lambda}_j^c$ are functions of the optimal \mathbf{x} in the form of (26) with their respective $\mathbf{D}(\mathbf{x})$ and \mathbf{A} matrices.

Proof: Based on Lemma 2, all the ratio functions in both the objective and the constraints are maximized with the same value for the variable \mathbf{z} , i.e., $\mathbf{z}^* = \mathbf{x}$. This must be the optimal solution of \mathbf{z} to the problem (42) because it not only maximizes the objective but also provides the largest constraint set of the variable \mathbf{x} . Substituting this optimal \mathbf{z}^* into (42) yields

$$\underset{\mathbf{x}, \boldsymbol{\lambda}_i^o, \boldsymbol{\lambda}_j^c}{\text{maximize}} \quad \sum_i w_i \bar{f}_i^o(\mathbf{x}, \mathbf{z}^*, \boldsymbol{\lambda}_i^o) = \sum_i w_i \tilde{f}_i^o(\mathbf{x}, \boldsymbol{\lambda}_i^o) \quad (43a)$$

$$\text{subject to} \quad \tilde{f}_j^c(\mathbf{x}, \mathbf{z}^*, \boldsymbol{\lambda}_j^c) = \tilde{f}_j^c(\mathbf{x}, \boldsymbol{\lambda}_j^c) \geq c_j, \quad \forall j, \quad (43b)$$

$$|x_n| = 1, \quad \forall n, \quad (43c)$$

where the quadratic functions $\tilde{f}_i^o(\mathbf{x}, \boldsymbol{\lambda}_i^o)$, $\tilde{f}_j^c(\mathbf{x}, \boldsymbol{\lambda}_j^c)$ are defined as in (25). The rest proof follows by invoking Theorem 2. ■

B. Reformulate (P1) via the Proposed Transform

Based on Theorem 3, problem (P1) is equivalent to

$$\text{(P3):} \quad \underset{\mathbf{x}, \mathbf{z}, \boldsymbol{\lambda}_r^o, \boldsymbol{\lambda}_k^c}{\text{maximize}} \quad \bar{\mathcal{A}}(\mathbf{x}, \mathbf{z}, \boldsymbol{\lambda}_r^o) \triangleq \sum_{r=1}^R \kappa_r \bar{f}_r^o(\mathbf{x}, \mathbf{z}, \boldsymbol{\lambda}_r^o) \quad (44a)$$

$$\text{subject to} \quad \bar{f}_k^c(\mathbf{x}, \mathbf{z}, \boldsymbol{\lambda}_k^c) \geq \Gamma_k, \quad \forall k, \quad (44b)$$

$$|x_n| = 1, \quad \forall n. \quad (44c)$$

The transformed functions in problem (P3) are given by

$$\begin{aligned} \bar{f}_r^o(\mathbf{x}, \mathbf{z}, \boldsymbol{\lambda}_r^o) = & 2 \Re \{ \mathbf{x}^H ((\delta_r^o \mathbf{I} - \mathbf{M}_r^o(\boldsymbol{\lambda}_r^o)) \mathbf{z} + \mathbf{R}_r^H \boldsymbol{\lambda}_r^o) \} + c_r^o(\mathbf{z}, \boldsymbol{\lambda}_r^o), \\ & (45) \end{aligned}$$

$$\begin{aligned} \bar{f}_k^c(\mathbf{x}, \mathbf{z}, \boldsymbol{\lambda}_k^c) = & 2 \Re \{ \mathbf{x}^H ((\delta_k^c \mathbf{I} - \mathbf{M}_k^c(\boldsymbol{\lambda}_k^c)) \mathbf{z} + \mathbf{H}_k^H \boldsymbol{\lambda}_k^c) \} + c_k^c(\mathbf{z}, \boldsymbol{\lambda}_k^c), \\ & (46) \end{aligned}$$

Algorithm 2 Linear Transform-Based Method

- 1: Initialize \mathbf{x} as a feasible point of the original problem (P1).
- 2: **repeat**
- 3: Update $\mathbf{z} = \mathbf{x}$.
- 4: Update $\boldsymbol{\lambda}_r^o = (\boldsymbol{\Sigma}^o(\mathbf{x}))^{-1} \mathbf{R}_r \mathbf{x}$ for all r .
- 5: Update $\boldsymbol{\lambda}_k^c = (\boldsymbol{\Sigma}_k^c(\mathbf{x}))^{-1} \mathbf{H}_k \mathbf{x}$ for all k .
- 6: Update \mathbf{x} by solving the subproblem (P4).
- 7: **until** convergence
- 8: **output** The optimized RIS reflecting coefficients \mathbf{x} .

where the matrices $\mathbf{M}_r^o(\boldsymbol{\lambda}_r^o)$ and $\mathbf{M}_k^c(\boldsymbol{\lambda}_k^c)$ are expressed in (33) and (36), respectively, δ_r^o and δ_k^c represents the traces of the matrices $\mathbf{M}_r^o(\boldsymbol{\lambda}_r^o)$ and $\mathbf{M}_k^c(\boldsymbol{\lambda}_k^c)$, respectively, and $c_r^o(\mathbf{z}, \boldsymbol{\lambda}_r^o)$ and $c_k^c(\mathbf{z}, \boldsymbol{\lambda}_k^c)$ are given by

$$c_r^o(\mathbf{z}, \boldsymbol{\lambda}_r^o) = \mathbf{z}^H \mathbf{M}_r^o(\boldsymbol{\lambda}_r^o) \mathbf{z} - 2\delta_r^o N - \sigma_n^2 \|\boldsymbol{\lambda}_r^o\|_2^2, \quad (47)$$

$$c_k^c(\mathbf{z}, \boldsymbol{\lambda}_k^c) = \mathbf{z}^H \mathbf{M}_k^c(\boldsymbol{\lambda}_k^c) \mathbf{z} - 2\delta_k^c N - \sigma_n^2 \|\boldsymbol{\lambda}_k^c\|_2^2. \quad (48)$$

Similar to problem (37), problem (P3) can be solved by iteratively updating the RIS beamforming vector and the auxiliary variables. When all the auxiliary variables are fixed, updating \mathbf{x} is an LP problem with constant-modulus constraints as

$$\text{(P4):} \quad \underset{\mathbf{x}}{\text{maximize}} \quad \sum_{r=1}^R \kappa_r \bar{f}_r^o(\mathbf{x}, \mathbf{z}, \boldsymbol{\lambda}_r^o) \quad (49a)$$

$$\text{subject to} \quad \bar{f}_k^c(\mathbf{x}, \mathbf{z}, \boldsymbol{\lambda}_k^c) \geq \Gamma_k, \quad \forall k, \quad (49b)$$

$$|x_n| = 1, \quad \forall n. \quad (49c)$$

When \mathbf{x} is held fixed, all the optimal auxiliary variables can be found in closed forms. The details are shown in Algorithm 2.

Note that the convergence of the proposed linear transform-based algorithm can be analyzed in a similar manner as that of Algorithm 1, and hence, it is omitted here. The convergence of Algorithm 2 to a KKT point of problem (P1) can be guaranteed if problem (P4) can be solved globally optimally. In the sequel, we show that the global optimality of problem (P4) can be achieved with linear complexity in the dimension of reflecting elements if certain conditions are satisfied.

C. Achieving Global Optimality of (P4)

The work [31] claims strong duality for an LP problem with constant-modulus constraints under certain conditions. In this subsection, we provide a similar but simpler proof for solving for the globally optimal solution for (P4). Consider first a relaxed version of (P4) obtained by replacing (49c) with the constraint $|x_n| \leq 1, \forall n$,

$$\underset{\mathbf{x}}{\text{maximize}} \quad \sum_{r=1}^R \kappa_r \bar{f}_r^o(\mathbf{x}, \mathbf{z}, \boldsymbol{\lambda}_r^o) \quad (50a)$$

$$\text{subject to} \quad \bar{f}_k^c(\mathbf{x}, \mathbf{z}, \boldsymbol{\lambda}_k^c) \geq \Gamma_k, \quad \forall k, \quad (50b)$$

$$|x_n| \leq 1, \quad \forall n. \quad (50c)$$

Note that the relaxed problem (50) is convex and enjoys strong duality. Its dual problem is given by

$$\underset{\boldsymbol{\nu} \geq \mathbf{0}}{\text{minimize}} \quad \max_{|x_n| \leq 1, \forall n} \mathcal{L}(\mathbf{x}, \boldsymbol{\nu}) \quad (51)$$

where $\boldsymbol{\nu} = [\nu_1, \dots, \nu_K]^\top$ denotes the dual variable associated with the linear constraints, and the partial Lagrangian is

$$\mathcal{L}(\mathbf{x}, \boldsymbol{\nu}) = \sum_{r=1}^R \kappa_r \bar{f}_r^o(\mathbf{x}, \mathbf{z}, \boldsymbol{\lambda}_r^o) + \sum_{k=1}^K \nu_k (\bar{f}_k^c(\mathbf{x}, \mathbf{z}, \boldsymbol{\lambda}_k^c) - \Gamma_k). \quad (52)$$

Since (52) is linear over \mathbf{x} , for fixed $\boldsymbol{\nu}$, the inner maximization in (51) is achieved if the elements of \mathbf{x} can be set to match the phases of the overall linear coefficient $\varsigma(\boldsymbol{\nu})$, i.e.,

$$\begin{aligned} \mathbf{x}(\boldsymbol{\nu}) &= \exp \left[j \arg \left(\sum_{r=1}^R \kappa_r \mathbf{d}_r^o + \sum_{k=1}^K \nu_k \mathbf{d}_k^c \right) \right] \\ &\triangleq \exp [j \arg (\varsigma(\boldsymbol{\nu}))], \end{aligned} \quad (53)$$

where \mathbf{d}_r^o and \mathbf{d}_k^c represent the liner coefficients in $\bar{f}_r^o(\mathbf{x}, \mathbf{z}, \boldsymbol{\lambda}_r^o)$ and $\bar{f}_k^c(\mathbf{x}, \mathbf{z}, \boldsymbol{\lambda}_k^c)$, respectively. In this case, the constraint $|x_n| \leq 1$ is achieved with equality. Thus, the dual for the relaxed problem attains the same optimal value as the problem below

$$\underset{\boldsymbol{\nu} \geq 0}{\text{minimize}} \quad \max_{|x_n|=1, \forall n} \mathcal{L}(\mathbf{x}, \boldsymbol{\nu}), \quad (54)$$

which is the dual problem of the original problem (P4). Since the optimal value of the dual problem is an upper bound to the optimal value of (P4), as long as this upper bound is achieved with x_n that satisfies the constraint $|x_n| = 1$, such x_n must be the global optimal solution to (P4).

It remains to check whether we can find a primal solution $\mathbf{x}(\boldsymbol{\nu})$ for the original problem (P4) that satisfies $|x_n| = 1$. Such a solution is given in (53), but it can be readily found if

$$[\varsigma(\boldsymbol{\nu}^*)]_n \neq 0, \quad \forall n, \quad (55)$$

where $\boldsymbol{\nu}^*$ denotes the optimal dual solution. Thus, if the above condition is satisfied, we get a global optimal solution to (P4). We summarize this statement below.

Proposition 1: If the optimal solution to the dual problem of (P4) $\boldsymbol{\nu}^*$ satisfies the condition (55), then the solution given by (53) is the global optimal solution of (P4).

This proposition provides a potential efficient method to obtain the globally optimal solution to (P4), even though (P4) is non-convex. Specifically, substituting $\mathbf{x}(\boldsymbol{\nu})$ in (53) into the dual objective function in (54), we obtain

$$\begin{aligned} \mathcal{L}(\mathbf{x}(\boldsymbol{\nu}), \boldsymbol{\nu}) &= 2 \left\| \sum_{r=1}^R \kappa_r \mathbf{d}_r^o + \sum_{k=1}^K \nu_k \mathbf{d}_k^c \right\|_1 + \sum_{r=1}^R \kappa_r c_r^o(\mathbf{z}, \boldsymbol{\lambda}_r^o) \\ &\quad + \sum_{k=1}^K \nu_k (c_k^c(\mathbf{z}, \boldsymbol{\lambda}_k^c) - \Gamma_k), \end{aligned} \quad (56)$$

which is convex on $\boldsymbol{\nu}$. In fact, the dual problem (54) is a linear programming problem, so it can be easily solved. Then, we verify whether the obtained $\boldsymbol{\nu}^*$ satisfies (55). If (55) is satisfied, the globally optimal solution of problem (P4) can be directly obtained by (53).

Empirically, for the scenario considered in this paper, where the number of reflecting elements are much greater than the number of users, the condition (55) is mostly satisfied in simulation. Similarly, [31] states in its appendix that it is quite rare to fail to meet this condition.

The per-iteration computational complexity of the algorithm proposed in this section is dominated by that of solving problem (54), which is polynomial with respect to the dimension of \mathbf{x} . This is the main advantage of the constant-modulus linear transform. Another advantage of the constant-modulus linear transform-based algorithm is that it is parameter-free, unlike the penalty quadratic transform-based algorithm, whose performance relies on the selection of the penalty coefficient.

VI. EXTENSION TO THE SCENARIO INVOLVING UNKNOWN FADING COEFFICIENT

In this section, we consider a more practical scenario where the fading coefficient α is unknown, but the goal remains to estimate the azimuth angle, because it is typically difficult to extract sensing information from the fading coefficient, which depends on the pathloss model, but such models are usually not known precisely [20]. We employ the modified BCRLB proposed in [32], which can be expressed as

$$\mathcal{B} \triangleq \mathbb{E}_{q(\alpha)} \left[\frac{1}{\mathbb{E}_{q(\eta|\alpha)} [\text{FI}(\eta|\alpha)] + \text{FIP}(\eta|\alpha)} \right], \quad (57)$$

where $\text{FI}(\eta|\alpha)$ denotes $\text{FI}(\eta)$ given α , and $\text{FIP}(\eta|\alpha)$ denotes $\text{FIP}(\eta)$ given α . Then, the problem of optimally designing the RIS beamforming vector for joint sensing and communications can be formulated as

$$(\mathbf{P5}): \quad \underset{\mathbf{x}}{\text{maximize}} \quad -\mathcal{B} \quad (58a)$$

$$\text{subject to} \quad \gamma_k \geq \Gamma, \quad \forall k, \quad (58b)$$

$$|x_n| = 1, \quad \forall n. \quad (58c)$$

If the distributions of α and η are independent, i.e., $q(\eta|\alpha) = q(\eta)$, which holds true at the initial sensing stage, the BCRLB can be rewritten as

$$\mathcal{B} = \mathbb{E}_{q(\alpha)} \left[\frac{1}{2p|\alpha|^2 \mathcal{A} + \text{FIP}(\eta)} \right]. \quad (59)$$

where \mathcal{A} is defined in (12). It can be observed from the above that minimizing \mathcal{B} is equivalent to maximizing \mathcal{A} since \mathcal{B} is a monotonically decreasing function of \mathcal{A} . Therefore, solving problem (P5) is similar to solving problem (P1).

A more challenging case arises when the distributions of α and η are not independent. Different from (12), the optimization variable \mathbf{x} cannot be separated from the expectations in (57), and Theorem 1 is no longer applicable. To tackle this challenge, we employ uniform sampling for approximating the expectations and rewrite \mathcal{B} as follows:

$$\mathcal{B} = \sum_{i=1}^S \frac{w_i}{\sum_{j=1}^L w_{i,j}^o \text{FI}(\eta_j|\alpha_i) + \text{FIP}(\eta|\alpha_i)}, \quad (60)$$

where S and L represent the number of sampling points for α and η , respectively, i, j , and t represent the indexes of samples, and $w_i = q(\alpha_i) / \sum_{t=1}^S q(\alpha_t)$, $w_{i,j}^o = q(\eta_j|\alpha_i) / \sum_{t=1}^L q(\eta_t|\alpha_i)$.

Clearly, $-\mathcal{B}$ is a non-decreasing function over each Fisher information term $\text{FI}(\eta_j|\alpha_i) \geq 0$. Before applying Theorem 2

to problem (P5), we first include an additional constraint into problem (P5) as follows:

$$\underset{\mathbf{x}}{\text{maximize}} \quad -\mathcal{B} \quad (61a)$$

$$\text{subject to} \quad \sum_{j=1}^L w_{i,j}^o \text{FI}(\eta_j|\alpha_i) + \text{FIP}(\eta|\alpha_i) \geq 0, \quad \forall i, \quad (61b)$$

$$\gamma_k \geq \Gamma, \quad \forall k, \quad (61c)$$

$$|x_n| = 1, \quad \forall n. \quad (61d)$$

The included constraint (61b) does not alter the constraint set since the Fisher information terms $\text{FI}(\eta_j|\alpha_i)$ and $\text{FIP}(\eta|\alpha_i)$ are always non-negative. But it needs to be included in order to ensure that the Fisher information terms remain nonnegative after the quadratic transform.

We now apply Theorem 2 to problem (61), yielding

$$\underset{\mathbf{x}, \boldsymbol{\lambda}_{i,j}^o, \boldsymbol{\lambda}_k^c}{\text{maximize}} \quad -\mathcal{C} \quad (62a)$$

$$\text{subject to} \quad \sum_{j=1}^L w_{i,j}^o \tilde{f}_{i,j}^o(\mathbf{x}, \boldsymbol{\lambda}_{i,j}^o) \geq -\text{FIP}(\eta|\alpha_i), \quad \forall i, \quad (62b)$$

$$\tilde{f}_k^c(\mathbf{x}, \boldsymbol{\lambda}_k^c) \geq \Gamma_k, \quad \forall k, \quad (62c)$$

$$|x_n| = 1, \quad \forall n, \quad (62d)$$

where the objective function \mathcal{C} is given by

$$\mathcal{C} = \sum_{i=1}^S \frac{w_i}{\sum_{j=1}^L 2pw_{i,j}^o \tilde{f}_{i,j}^o(\mathbf{x}, \boldsymbol{\lambda}_{i,j}^o) + \text{FIP}(\eta|\alpha_i)}, \quad (63)$$

and the constraint functions $\tilde{f}_k^c(\mathbf{x}, \boldsymbol{\lambda}_k^c)$ are given in (31). The transformed function $\tilde{f}_{i,j}^o(\mathbf{x}, \boldsymbol{\lambda}_{i,j}^o)$ in (63) is given by

$$\begin{aligned} \tilde{f}_{i,j}^o(\mathbf{x}, \boldsymbol{\lambda}_{i,j}^o) &= 2 \Re \left\{ (\boldsymbol{\lambda}_{i,j}^o)^H \left(\alpha_i \hat{\mathbf{U}}(\eta_j) \mathbf{x} \right) \right\} - (\boldsymbol{\lambda}_{i,j}^o)^H \Sigma^o(\mathbf{x}) \boldsymbol{\lambda}_{i,j}^o. \end{aligned} \quad (64)$$

Clearly, the objective function $-\mathcal{C}$ is concave over \mathbf{x} .

Then, utilizing the penalty-based approach in Section IV-B, the problem (62) can be further transformed into

$$\underset{\mathbf{x}, \mathbf{z}, \boldsymbol{\lambda}_{i,j}^o, \boldsymbol{\lambda}_k^c}{\text{maximize}} \quad -\mathcal{C} - \mu \|\mathbf{x} - \mathbf{z}\|_2^2 \quad (65a)$$

$$\text{subject to} \quad \sum_{j=1}^L w_{i,j}^o \tilde{f}_{i,j}^o(\mathbf{x}, \boldsymbol{\lambda}_{i,j}^o) \geq -\text{FIP}(\eta|\alpha_i), \quad \forall i, \quad (65b)$$

$$\tilde{f}_k^c(\mathbf{x}, \boldsymbol{\lambda}_k^c) \geq \Gamma_k, \quad \forall k, \quad (65c)$$

$$|x_n| \leq 1, \quad \forall n. \quad (65d)$$

Similar to the problem (37), the above problem can be solved by iteratively optimizing the RIS beamforming vector and all the auxiliary variables. The details are omitted here.

VII. NUMERICAL RESULTS

In this section, we provide the numerical results to show the effectiveness of the proposed algorithms for RIS-assisted joint sensing and communication. The simulation environment is set as follows.

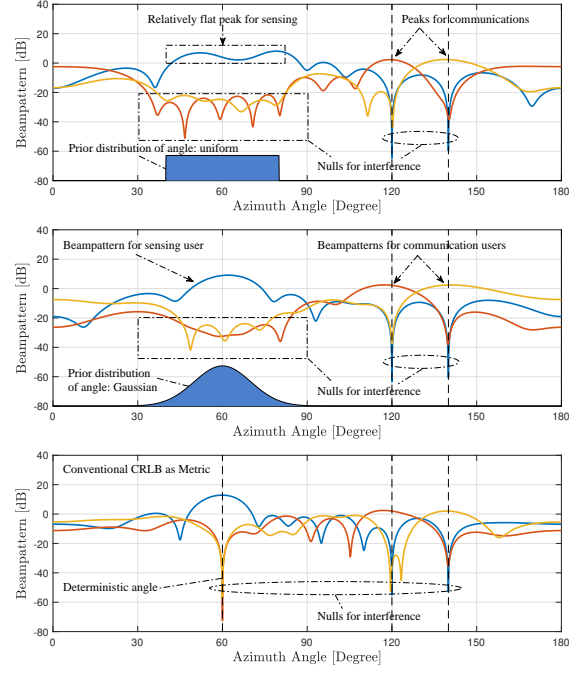


Fig. 2. RIS reflecting beampatterns with different prior distributions of the azimuth angle of sensing user.

- The distance between the BS and the RIS is 100 meters and the distance between the users and the RIS is 20 meters.
- Considering the relatively large distance and the random scattering between the RIS and the BS, the RIS-BS channel is modeled as a Rayleigh fading channel. For the user-RIS links, we use a Rician fading model with K -factor of $+\infty$, i.e., with LoS path only.
- The path-loss of the user-RIS path and the RIS-BS path are respectively set to be

$$-30 - 20 \log(20) = -56 \text{ dB}, \quad (66)$$

$$-30 - 20 \log(100) = -70 \text{ dB}. \quad (67)$$

- The BS is equipped with 8 antennas, which are arranged in a uniform linear array. The RIS is a planar with 8×8 or 10×10 reflecting elements. Both the spacing between the antennas and the reflecting elements are half wavelength.
- The transmit power of each user is set to be 10 dBm, the noise power at the BS is set up as -100 dBm, and the SINR threshold is set to be 15 dB.
- We use the CVX with MOSEK as the optimization solver to handle the convex optimization problem involved in the optimization process.

A. RIS Reflecting Beampatterns

We use the beampatterns to illustrate the effectiveness of the proposed algorithms. This subsection presents the beampattern

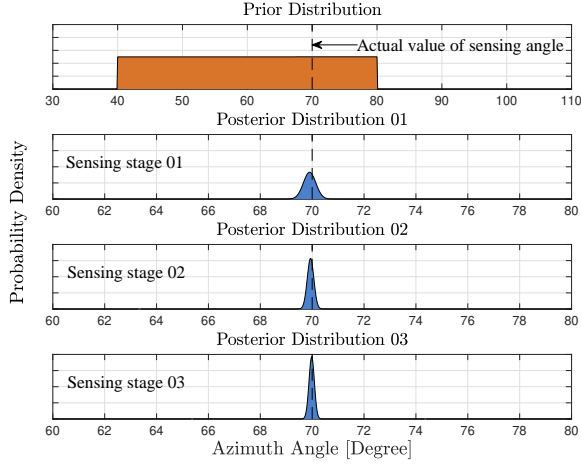


Fig. 3. Posterior distributions of the angle η over three iterations with adaptive RIS sensing (fading coefficient α is known).

for the case where α is known; the beampattern for the case where α is unknown is similar.

The RIS beampattern for the k -th communication user is defined as follows:

$$\mathcal{Q}_k = |\mathbf{w}_k^H (\mathbf{G} \Phi \mathbf{v}(\phi))|^2, \quad (68)$$

which is the received signal power after linear minimum mean square error (LMMSE) combining at the BS from a unit-power transmitter at an azimuth angle ϕ with respect to the RIS.

Although received combiner is generally not used for sensing, for comparison purpose, we also plot the received signal power for the sensing user by using a linear combiner \mathbf{w} similar for the communication users as given below:

$$\mathbf{w} = \delta_{\max} \left((\Sigma^o(\mathbf{x}))^{-1} \mathbb{E}_{q(\eta)} \left[(\mathbf{U}(\eta)\mathbf{x}) (\mathbf{U}(\eta)\mathbf{x})^H \right] \right), \quad (69)$$

where $\delta_{\max}(\mathbf{A})$ denotes the eigenvector corresponding to the largest eigenvalue of \mathbf{A} . Specifically, we consider three scenarios:

- 1) The azimuth angle η of the sensing user has a uniform prior distribution in the range $[40^\circ, 80^\circ]$.
- 2) The azimuth angle η has a Gaussian prior distribution with mean 60° and standard deviation 10° .
- 3) The azimuth angle η is deterministic at 60° .

All the above scenarios have two communication users at 120° and 140° , respectively.

The designed RIS reflecting beampatterns have intuitive interpretation. From Fig. 2, it can be observed that the solutions of the beam-forming optimization problem produce beams that are aligned with the directions of communication users, while also having a peak matching the prior distribution of the sensing angle. In addition, the nulls of the beampatterns are also aligned with the directions of interference, especially the nulls of beampatterns for communication users are aligned with the prior distribution of the sensing angle. These aligned peaks and nulls help improve the performance of joint sensing and communication.

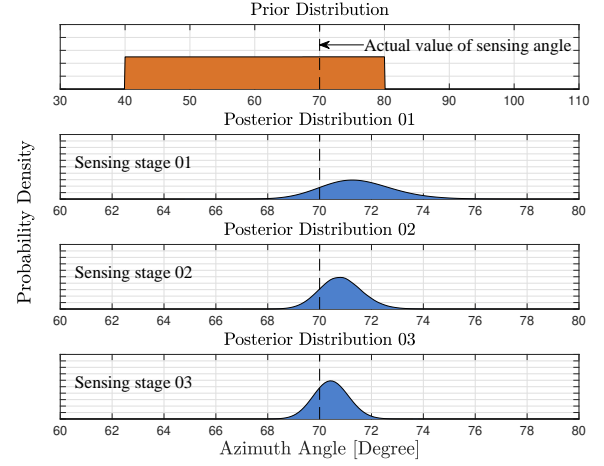


Fig. 4. Posterior distributions of the angle η over three iterations with adaptive RIS sensing (fading coefficient α is unknown).

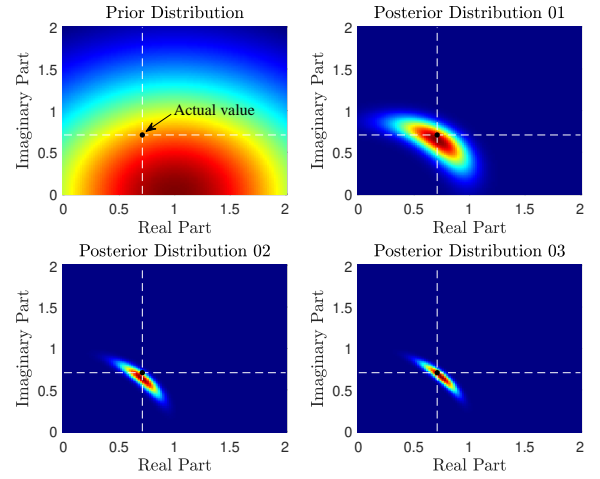


Fig. 5. Posterior distributions of the fading coefficient α over three iterations with adaptive RIS sensing.

B. Posterior Distributions of Estimated Parameters

To further illustrate the sensing performance of the proposed algorithms, we present evolution of the posterior distributions after several iterations of sensing stages in Figs. 3–5. First, we consider the case where α is known. The posterior probability function of the $(t+1)$ -th sensing stage is computed as follows. Note that the communication signals are regarded as noise for sensing. In this case, we have

$$\begin{aligned} \Pr(\eta | \mathbf{y}_{t+1}) &\propto \mathcal{L}(\mathbf{y}_{t+1}; \eta) \cdot \Pr(\eta | \mathbf{y}_t) \\ &= \mathcal{CN}(\text{mean}(\mathbf{y}_{t+1} | \eta), \text{Cov}(\mathbf{y}_{t+1} | \eta)) \cdot \Pr(\eta | \mathbf{y}_t), \end{aligned} \quad (70)$$

where $\mathcal{L}(\mathbf{y}_{t+1} | \eta)$ is the Gaussian likelihood function with the mean and covariance matrix given in (8) and (9), respectively, and $\Pr(\eta | \mathbf{y}_t)$ denotes the posterior distribution from the previous iteration, which is adopted as the prior distribution $q(\eta)$ for the current iteration. Then, the above process can be repeated until the accuracy of angle estimation satisfies the requirement.

We show the results of the first scenario of Fig. 2, where the fading coefficient α is known, and the azimuth angle η has a uniform distribution in the range $[40^\circ, 80^\circ]$. The actual angle of the sensing user is set to be 70° . The communication signals are randomly generated from a Gaussian distribution. The pilot signal for the sensing user is a known sequence with transmit power $p = 10$ dBm. In Fig. 3, we plot the posterior distribution of η after three iterations using the RIS beamforming vectors designed by our proposed algorithms. From Fig. 3, it can be seen that as the number of iterations increases, the posterior distribution rapidly converges to a highly concentrated distribution with a peak at the true sensing angle. This shows that the proposed beamforming design is highly effective for sensing.

In Figs. 4 and 5, we plot the result for the scenario where the fading coefficient α is unknown. The prior distribution of α is set as $(-56 \text{ dB}) \times \mathcal{CN}(1, 1)$, and the actual value of α is set as $(-56 \text{ dB}) \times (0.7 + 0.7j)$. In this case, the posterior distribution is modified as follows:

$$\begin{aligned} \Pr(\eta, \alpha | \mathbf{y}_{t+1}) &\propto \mathcal{L}(\mathbf{y}_{t+1}; \eta, \alpha) \cdot \Pr(\eta, \alpha | \mathbf{y}_t) \\ &= \mathcal{CN}(\text{mean}(\mathbf{y}_{t+1} | \eta, \alpha), \text{Cov}(\mathbf{y}_{t+1} | \eta, \alpha)) \cdot \Pr(\eta, \alpha | \mathbf{y}_t), \end{aligned} \quad (71)$$

and the posterior distributions of α and η can be computed by $\int_{\eta} \Pr(\eta, \alpha | \mathbf{y}_{t+1})$ and $\int_{\alpha} \Pr(\eta, \alpha | \mathbf{y}_{t+1})$, respectively. One can observe from Figs. 4 and 5 that with increasing number of iterations, both the posterior distributions of α and η rapidly converge to a concentrated distribution. This shows that the proposed beamforming design is highly effective for sensing. However, compared to Fig. 3, i.e., the case where α is already known, the convergence rate in Fig. 4 is slower, reflecting the impact of uncertainty in fading coefficient on angle estimation.

C. Estimation and Optimization Performance

We now show the performance achieved by using the BCRLB as sensing metric as compared to using the classic CRLB. Consider the first scenario of Fig. 2, i.e., the azimuth angle of sensing user is uniformly distributed in the range of $[40^\circ, 80^\circ]$. The actual azimuth angle of the sensing user is at 70° . The classic CRLB computation relies on the exact value of η , which is unknown and needs to be estimated. One possible approach is to use the mean of η to compute the CRLB. In contrast, the BCRLB utilizes the prior distribution of η . For both cases, maximum a posteriori (MAP) estimation is used to estimate the azimuth angle of the sensing user, i.e.,

$$\hat{\eta} = \arg \max_{\eta} \Pr(\eta | \mathbf{y}), \quad (\hat{\eta}, \hat{\alpha}) = \arg \max_{\eta, \alpha} \Pr(\eta, \alpha | \mathbf{y}), \quad (72)$$

where the posterior distributions are given in (70) and (71). The MSE of estimation is estimated via 5,000 Monte-Carlo trials with randomly generated noise and data symbols.

In Fig. 6, we plot the CRLB and the MSE of estimating the angle $\eta = 70^\circ$ with different RIS beamformers designed by optimizing different sensing metrics. We also plot the results of the all-one RIS beamformer. One can observe from Fig. 6 that adopting the BCRLB as the sensing metric can provide much better estimation performance than that of using the CRLB as the sensing metric. The gain is approximately 5.76 dB. Moreover, when the transmit power is low, e.g., 10

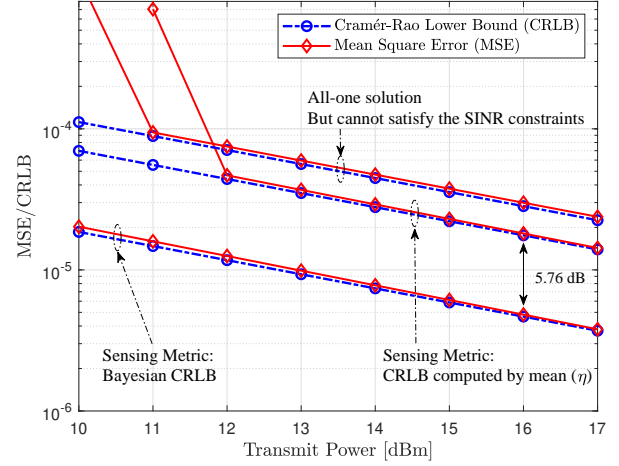


Fig. 6. Mean square error and Cramér-Rao lower bound of angle estimation with different RIS beamformers (fading coefficient α is known).

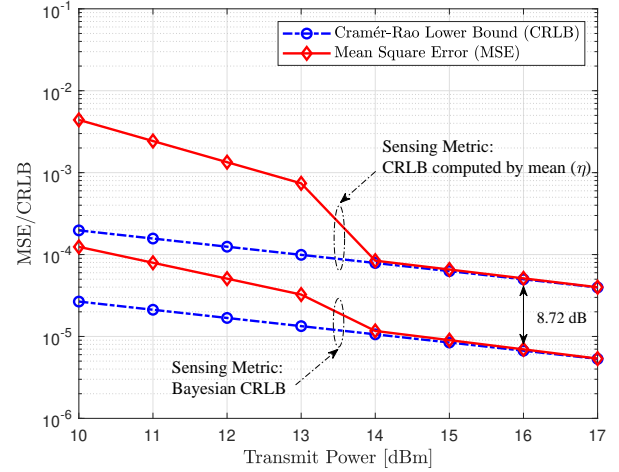


Fig. 7. Mean square error and Cramér-Rao lower bound of angle estimation with different RIS beamformers (fading coefficient α is unknown).

and 11 dBm, using the BCRLB as the sensing metric can provide a tighter bound for MSE than that of using the CRLB as the metric and the all-one RIS beamformer.

In Fig. 7, we consider the same setup with Fig. 6, but with an unknown fading coefficient α . The prior distribution of α is set up as $(-56 \text{ dB}) \times \mathcal{CN}(1, 1)$. From Fig. 7, in addition to observing results similar to those in Fig. 6, it can be observed that both the MSE and CRLB are higher than that in Fig. 6, reflecting the impact of uncertainty in α on angle estimation. It can also be observed that when the transmit power is low, the classic CRLB is not tight. This is because the estimation performance is particularly sensitive to the power of received signals in this case, making the estimation performance worse.

Next, we show the optimization performance of the proposed algorithms. To the best of our knowledge, no prior work has considered the FCFP beamforming problem solved in this paper. Thus, we utilize an interior-point like benchmark to handle the SINR constraints and then employ the projected

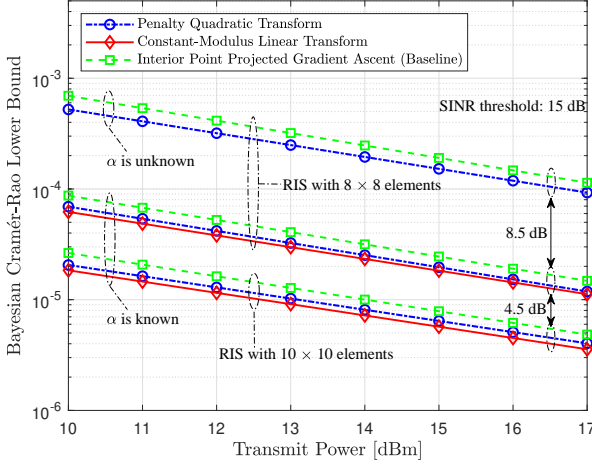


Fig. 8. Bayesian Cramér-Rao lower bound versus the transmit power using different algorithms and with different numbers of RIS elements.

gradient ascent method to solve the following problem:

$$\underset{|x_n|=1}{\text{maximize}} \quad \text{Obj}(\mathbf{x}) + \sum_{k=1}^K \frac{1}{\mu} \log(\gamma_k - \Gamma). \quad (73)$$

Fig. 8 plots the optimized BCRLB versus the transmit power. One can observe that the proposed algorithms perform better than the projected gradient ascent benchmark algorithm, which validates the proposed algorithms. If the number of reflecting elements increases from 8×8 to 10×10 , an approximate gain of 4.5 dB is observed. Moreover, for fixed 8×8 reflecting elements at RIS, the uncertainty of α results in a loss of approximately 8.5 dB.

VIII. CONCLUSION

This paper proposes a methodology for RIS beamforming pattern design for an uplink RIS-assisted integrated sensing and communications scenario. We formulate the optimization problem of minimizing the BCRLB of azimuth angle estimation for the sensing user, while imposing SINR constraints for multiple communication users. This problem is a non-convex fractional program with fractional constraints. We utilize two transform techniques to deal with the fractional structures in both the objective function and the constraints, which turn the problem into a sequence of convex subproblems. Simulation results demonstrate highly effective RIS beampattern design for both sensing and communications.

APPENDIX A PROOF OF THEOREM 1

Since $\Sigma^0(\mathbf{x})$ is a positive definite matrix, we can decompose its inverse as $(\Sigma^0(\mathbf{x}))^{-1} = \Upsilon^H \Upsilon$. According to the properties of the Kronecker product, given matrices \mathbf{A} , \mathbf{B} , \mathbf{C} , and \mathbf{D} , we have

$$\text{vec}(\mathbf{ACB}) = (\mathbf{B}^T \otimes \mathbf{A}) \text{vec}(\mathbf{C}), \quad (74)$$

$$(\mathbf{A} \otimes \mathbf{B})(\mathbf{C} \otimes \mathbf{D}) = (\mathbf{AC}) \otimes (\mathbf{BD}). \quad (75)$$

Then, the inner part of (12) can be rewritten as follows:

$$\begin{aligned} & (\dot{\mathbf{U}}(\eta)\mathbf{x})^H (\Sigma^0(\mathbf{x}))^{-1} (\dot{\mathbf{U}}(\eta)\mathbf{x}) = (\Upsilon \dot{\mathbf{U}}(\eta)\mathbf{x})^H (\Upsilon \dot{\mathbf{U}}(\eta)\mathbf{x}) \\ & = ((\mathbf{x}^T \otimes \Upsilon) \text{vec}(\dot{\mathbf{U}}(\eta)))^H ((\mathbf{x}^T \otimes \Upsilon) \text{vec}(\dot{\mathbf{U}}(\eta))) \\ & = \text{vec}^H(\dot{\mathbf{U}}(\eta)) (\mathbf{x}^* \otimes \Upsilon^H) (\mathbf{x}^T \otimes \Upsilon) \text{vec}(\dot{\mathbf{U}}(\eta)) \\ & = \text{vec}^H(\dot{\mathbf{U}}(\eta)) (\mathbf{x}^* \mathbf{x}^T \otimes \Upsilon^H \Upsilon) \text{vec}(\dot{\mathbf{U}}(\eta)) \\ & = \text{Tr}((\mathbf{x}^* \mathbf{x}^T \otimes (\Sigma^0(\mathbf{x}))^{-1}) (\text{vec}(\dot{\mathbf{U}}(\eta)) \text{vec}^H(\dot{\mathbf{U}}(\eta)))). \end{aligned} \quad (76)$$

Thus, the expectation in (12) can be equivalently rewritten as

$$\mathcal{A} = \text{Tr} \left((\mathbf{x}^* \mathbf{x}^T \otimes (\Sigma^0(\mathbf{x}))^{-1}) \dot{\mathbf{R}} \right), \quad (77)$$

where $\dot{\mathbf{R}}$ is the expectation given in (13). Since $\dot{\mathbf{R}}$ is a positive semidefinite matrix, it has an eigenvalue decomposition as

$$\dot{\mathbf{R}} = \sum_{r=1}^R \kappa_r \mathbf{r}_r \mathbf{r}_r^H, \quad (78)$$

where κ_r and \mathbf{r}_r are the r -th eigenvalue and the corresponding eigenvector of $\dot{\mathbf{R}}$, respectively. Then, substituting (78) into (77) and applying the derivation in (76) in reverse give us (15).

APPENDIX B PROOF OF THEOREM 2

First, we show that the problem (28) is equivalent to

$$\begin{aligned} & \underset{\mathbf{x} \in \mathcal{X}}{\text{maximize}} \quad h^0 \left(\max_{\lambda_1^0} \tilde{f}_1^0(\mathbf{x}, \lambda_1^0), \dots, \max_{\lambda_I^0} \tilde{f}_I^0(\mathbf{x}, \lambda_I^0) \right) \quad (79a) \\ & \text{subject to} \quad h_k^c \left(\max_{\lambda_{k,1}^c} \tilde{f}_{k,1}^c(\mathbf{x}, \lambda_{k,1}^c), \dots, \max_{\lambda_{k,J}^c} \tilde{f}_{k,J}^c(\mathbf{x}, \lambda_{k,J}^c) \right) \\ & \quad \geq c_k, \quad \forall k. \quad (79b) \end{aligned}$$

The equivalence between the objectives of the two problems is due to that the outer function h^0 is non-decreasing in each component, and the auxiliary variables λ_i^0 are separable, so

$$\begin{aligned} & \underset{\mathbf{x} \in \mathcal{X}, \lambda_i^0, \lambda_j^c}{\text{maximize}} \quad h^0 \left(\tilde{f}_1^0(\mathbf{x}, \lambda_1^0), \dots, \tilde{f}_I^0(\mathbf{x}, \lambda_I^0) \right) = \\ & \underset{\mathbf{x} \in \mathcal{X}}{\text{maximize}} \quad h^0 \left(\max_{\lambda_1^0} \tilde{f}_1^0(\mathbf{x}, \lambda_1^0), \dots, \max_{\lambda_I^0} \tilde{f}_I^0(\mathbf{x}, \lambda_I^0) \right). \quad (80) \end{aligned}$$

Next, we show that the feasible set of \mathbf{x} satisfying (79b) is the same as that satisfying (28b). Let $(\mathbf{x}, \{\lambda_{k,j}^c\})$ be a point satisfying (28b). Then, \mathbf{x} must satisfy (79b) since the latter constraint maximizes $\tilde{f}_{k,j}^c(\mathbf{x}, \lambda_{k,j}^c)$ over $\lambda_{k,j}^c$ in each component and the outer function h_k^c is non-decreasing in each component. Conversely, if \mathbf{x} is a feasible point in (79b), $(\mathbf{x}, \{(\lambda_{k,j}^c)^*\})$ is a feasible point in (28b), where $(\lambda_{k,j}^c)^* = \arg \max_{\lambda_{k,j}^c} \tilde{f}_{k,j}^c(\mathbf{x}, \lambda_{k,j}^c)$. Hence, the feasible set of \mathbf{x} in the problem (28) is the same as that in the problem (79). Combined with the fact that the two objectives are equal, this shows that the two problems are equivalent.

Second, we show the equivalence between the problems (79) and (27). Based on Lemma 1, we have

$$\max_{\lambda_i^0} \tilde{f}_i^0(\mathbf{x}, \lambda_i^0) = f_i^0(\mathbf{x}), \quad (81)$$

$$\max_{\lambda_{k,j}^c} \tilde{f}_{k,j}^c(\mathbf{x}, \lambda_{k,j}^c) = f_{k,j}^c(\mathbf{x}). \quad (82)$$

Therefore, the problem (79) is equivalent to the problem (27) since both the objective function and the constraints are the same. Finally, combined with the fact that the problem (28) is equivalent to the problem (79), the problem (28) is equivalent to the problem (27).

APPENDIX C PROOF OF LEMMA 2

Based on Lemma 1, we have the following relation:

$$f(\mathbf{x}) \geq 2\Re(\lambda^H \mathbf{A}\mathbf{x}) - \lambda^H \mathbf{D}(\mathbf{x})\lambda. \quad (83)$$

The second term in (83) can be rewritten as

$$\begin{aligned} \lambda^H \mathbf{D}(\mathbf{x})\lambda &= \mathbf{x}^H \left(\sum_m (\mathbf{B}_m^H \lambda) (\mathbf{B}_m^H \lambda)^H \right) \mathbf{x} + \lambda^H \mathbf{C}\lambda \\ &\triangleq \mathbf{x}^H \mathbf{M}(\lambda)\mathbf{x} + \lambda^H \mathbf{C}\lambda. \end{aligned} \quad (84)$$

Then, we eliminate the quadratic term in (84) by making use of the fact that for unit-modulus variables \mathbf{x} and \mathbf{z} ,

$$\mathbf{x}^H (\delta \mathbf{I}) \mathbf{x} = \mathbf{z}^H (\delta \mathbf{I}) \mathbf{z} = \delta N. \quad (85)$$

Specifically, we apply (26) in [33] to (84), which is given by

$$\begin{aligned} \mathbf{x}^H \mathbf{M}(\lambda)\mathbf{x} &\leq \mathbf{x}^H \mathbf{L}\mathbf{x} + \mathbf{z}^H (\mathbf{L} - \mathbf{M}(\lambda)) \mathbf{z} \\ &\quad + 2\Re(\mathbf{x}^H (\mathbf{M}(\lambda) - \mathbf{L}) \mathbf{z}), \end{aligned} \quad (86)$$

where $\mathbf{L} \succeq \mathbf{M}(\lambda)$ and the equality is achieved at $\mathbf{z} = \mathbf{x}$. Then, by replacing \mathbf{L} with $\delta \mathbf{I}$, where δ is the trace of $\mathbf{M}(\lambda)$ so that $\delta \mathbf{I} \succeq \mathbf{M}(\lambda)$, and by combining with (83), we obtain

$$\begin{aligned} f(\mathbf{x}) &\geq 2\Re(\mathbf{x}^H ((\delta \mathbf{I} - \mathbf{M}(\lambda)) \mathbf{z} + \mathbf{A}^H \lambda)) + c(\mathbf{z}, \lambda) \\ &\triangleq \bar{f}(\mathbf{x}, \mathbf{z}, \lambda), \end{aligned} \quad (87)$$

where $c(\mathbf{z}, \lambda)$ is given in (40). The equality in the above is achieved when $\mathbf{z} = \mathbf{x}$ and $\lambda = (\mathbf{D}(\mathbf{x}))^{-1} \mathbf{A}\mathbf{x}$.

REFERENCES

- [1] Y. Liu and W. Yu, "RIS-assisted joint sensing and communications via fractionally constrained fractional programming," in *Prof. IEEE Global Commun. Conf. (GLOBECOM)*, Cape Town, South Africa, Dec. 2024.
- [2] F. Liu, Y. Cui, C. Masouros, J. Xu, T. X. Han, Y. C. Eldar, and S. Buzzi, "Integrated sensing and communications: Toward dual-functional wireless networks for 6G and beyond," *IEEE J. Sel. Areas Commun.*, vol. 40, no. 6, pp. 1728–1767, Jun. 2022.
- [3] J. A. Zhang, F. Liu, C. Masouros, R. W. Heath, Z. Feng, L. Zheng, and A. Petropulu, "An overview of signal processing techniques for joint communication and radar sensing," *IEEE J. Sel. Topics Signal Process.*, vol. 15, no. 6, pp. 1295–1315, Nov. 2021.
- [4] Y. Cui, F. Liu, X. Jing, and J. Mu, "Integrating sensing and communications for ubiquitous IoT: Applications, trends, and challenges," *IEEE Netw.*, vol. 35, no. 5, pp. 158–167, Sep./Oct. 2021.
- [5] C. Huang, A. Zappone, G. C. Alexandropoulos, M. Debbah, and C. Yuen, "Reconfigurable intelligent surfaces for energy efficiency in wireless communication," *IEEE Trans. Wireless Commun.*, vol. 18, no. 8, pp. 4157–4170, Aug. 2019.
- [6] Q. Wu and R. Zhang, "Intelligent reflecting surface enhanced wireless network via joint active and passive beamforming," *IEEE Trans. Wireless Commun.*, vol. 18, no. 11, pp. 5394–5409, Nov. 2019.
- [7] S. P. Chepuri, N. Shlezinger, F. Liu, G. C. Alexandropoulos, S. Buzzi, and Y. C. Eldar, "Integrated sensing and communications with reconfigurable intelligent surfaces: From signal modeling to processing," *IEEE Signal Process. Mag.*, vol. 40, no. 6, pp. 41–62, Sep. 2023.
- [8] F. Liu, L. Zhou, C. Masouros, A. Li, W. Luo, and A. Petropulu, "Toward dual-functional radar-communication systems: Optimal waveform design," *IEEE Trans. Signal Process.*, vol. 66, no. 16, pp. 4264–4279, Aug. 2018.
- [9] X. Liu, T. Huang, N. Shlezinger, Y. Liu, J. Zhou, and Y. C. Eldar, "Joint transmit beamforming for multiuser MIMO communications and MIMO radar," *IEEE Trans. Signal Process.*, vol. 68, pp. 3929–3944, 2020.
- [10] X. Shao, C. You, W. Ma, X. Chen, and R. Zhang, "Target sensing with intelligent reflecting surface: Architecture and performance," *IEEE J. Sel. Areas Commun.*, vol. 40, no. 7, pp. 2070–2084, Jul. 2022.
- [11] W. Lu, Q. Lin, N. Song, Q. Fang, X. Hua, and B. Deng, "Target detection in intelligent reflecting surface aided distributed MIMO radar systems," *IEEE Sens. Lett.*, vol. 5, no. 3, pp. 1–4, Mar. 2021.
- [12] S. Buzzi, E. Grossi, M. Lops, and L. Venturino, "Radar target detection aided by reconfigurable intelligent surfaces," *IEEE Signal Process. Lett.*, vol. 28, pp. 1315–1319, 2021.
- [13] —, "Foundations of MIMO radar detection aided by reconfigurable intelligent surfaces," *IEEE Trans. Signal Process.*, vol. 70, pp. 1749–1763, 2022.
- [14] R. Liu, M. Li, Y. Liu, Q. Wu, and Q. Liu, "Joint transmit waveform and passive beamforming design for RIS-aided DFRC systems," *IEEE J. Sel. Topics Signal Process.*, vol. 16, no. 5, pp. 995–1010, Aug. 2022.
- [15] R. Liu, M. Li, Q. Liu, and A. Lee Swindlehurst, "SNR/CRB-constrained joint beamforming and reflection designs for RIS-ISAC systems," *IEEE Trans. Wireless Commun.*, vol. 23, no. 7, pp. 7456–7470, Jul. 2024.
- [16] Z.-M. Jiang, M. Rihan, P. Zhang, L. Huang, Q. Deng, J. Zhang, and E. M. Mohamed, "Intelligent reflecting surface aided dual-function radar and communication system," *IEEE Syst. J.*, vol. 16, no. 1, pp. 475–486, Mar. 2022.
- [17] E. Grossi, H. Taremi-zadeh, and L. Venturino, "Radar target detection and localization aided by an active reconfigurable intelligent surface," *IEEE Signal Process. Lett.*, vol. 30, pp. 903–907, 2023.
- [18] Y. Liu, E. Liu, R. Wang, and Y. Geng, "Reconfigurable intelligent surface aided wireless localization," in *Prof. IEEE Int. Conf. Commun.*, Montreal, Canada, Jun. 2021, pp. 1–6.
- [19] F. Liu, Y.-F. Liu, A. Li, C. Masouros, and Y. C. Eldar, "Cramér-Rao bound optimization for joint radar-communication beamforming," *IEEE Trans. Signal Process.*, vol. 70, pp. 240–253, 2022.
- [20] X. Song, J. Xu, F. Liu, T. X. Han, and Y. C. Eldar, "Intelligent reflecting surface enabled sensing: Cramér-Rao bound optimization," *IEEE Trans. Signal Process.*, vol. 71, pp. 2011–2026, 2023.
- [21] X. Song, X. Qin, J. Xu, and R. Zhang, "Cramér-Rao bound minimization for IRS-enabled multiuser integrated sensing and communications," *IEEE Trans. Wireless Commun.*, vol. 23, no. 8, pp. 9714–9729, Aug. 2024.
- [22] W. Huleihel, J. Tabrikian, and R. Shavit, "Optimal adaptive waveform design for cognitive mimo radar," *IEEE Trans. Signal Processing*, vol. 61, no. 20, pp. 5075–5089, 2013.
- [23] K. Shen and W. Yu, "Fractional programming for communication systems—Part I: Power control and beamforming," *IEEE Trans. Signal Process.*, vol. 66, no. 10, May 2018.
- [24] B. Zheng, C. You, W. Mei, and R. Zhang, "A survey on channel estimation and practical passive beamforming design for intelligent reflecting surface aided wireless communications," *IEEE Commun. Surv. Tutor.*, vol. 24, no. 2, pp. 1035–1071, Feb. 2022.
- [25] A. Alkhateeb, O. El Ayach, G. Leus, and R. W. Heath, "Channel estimation and hybrid precoding for millimeter wave cellular systems," *IEEE J. Sel. Topics Signal Process.*, vol. 8, no. 5, pp. 831–846, Oct. 2014.
- [26] S. M. Kay, *Fundamentals of Statistical Signal Processing: Estimation Theory*. Englewood Cliffs, NJ: PTR Prentice Hall, 1993.
- [27] H. L. Van Trees, *Optimum Array Processing: Part IV of Detection, Estimation, and Modulation Theory*. Hoboken, NJ, USA: Wiley, 2002.
- [28] J. Dauwels, "Computing Bayesian Cramer-Rao bounds," in *Proc. IEEE Int. Symp. Inf. Theory (ISIT)*, Sept. 2005, pp. 425–429.
- [29] C. Xu and S. Zhang, "MIMO integrated sensing and communication exploiting prior information," *IEEE J. Sel. Areas Commun.*, pp. 1–1, 2024.
- [30] I. Bekkerman and J. Tabrikian, "Target detection and localization using MIMO radars and sonars," *IEEE Trans. Signal Process.*, vol. 54, no. 10, pp. 3873–3883, 2006.
- [31] X. He and J. Wang, "QCCP with extra constant modulus constraints: Theory and application to SINR constrained mmwave hybrid beamforming," *IEEE Trans. Signal Process.*, vol. 70, pp. 5237–5250, Oct. 2022.
- [32] R. Miller and C. Chang, "A modified Cramér-Rao bound and its applications," *IEEE Trans. Inf. Theory*, vol. 24, no. 3, pp. 398–400, May 1978.
- [33] Y. Sun, P. Babu, and D. P. Palomar, "Majorization-minimization algorithms in signal processing, communications, and machine learning," *IEEE Trans. Signal Process.*, vol. 65, no. 3, pp. 794–816, Feb. 2017.